A multi-purpose cryogenic test facility for astronomical instrumentation

Stephen A. March[a], Adrian M. Glauser[a], Marcel Baer[a], and Polychronis Patapis[a]

[a]ETH Zurich, Department of Physics, Zurich, Switzerland

ABSTRACT

We present the design, capabilities and applications of a cryogenic test facility for astronomical instrumentation located at ETH Zurich, Switzerland. This facility was designed, built, and commissioned with the purpose to support opto-mechanical performance measurements of cryo-mechanisms for astronomical instruments. In particular, the facility was developed initially to test the opto-mechanical stability and repeatability of the wheel-mechanisms for the ERIS/VLT instrument that are developed in house. However, the facility has a generic application portfolio and can be used for other development projects as well. The unique setup allows optical access from the warm end with short working distance to the cold elements of only a few millimeters. Electrical, mechanical, and liquid feedthroughs provide a flexible infrastructure for a large variety of thermal, mechanical, electrical and optical tests. To provide maximum mechanical stability, the cooling is provided by a low vibration pulse tube cooler that cools the facility down to approximately 8 K.

Keywords: cryogenics, test facility, cryocooler, instrumentation, cryo-mechanism

1. DESIGN OVERVIEW

The primary purpose of this lab cryostat was for performance tests of the Pupil- and Filter-Wheel and the Aperture-Wheel mechanisms for the NIX camera of the VLT/ERIS instrument.[1] For this a test temperature of 70 K and low vibration environment was required. The tests were performed using a setup that could measure to a few microns using a camera with a macro lens, however, the short working distance of 100 mm meant that there was limited space and so the resulting cryostat design had less than 2 cm between the outside of the warm window and the inside of the cold box.

An overview of the cryostat is shown in Figure 1. The sample chamber (cold box) is approximately 400 mm by 400 mm by 400 mm and was designed to work down to about 10 K, in order to test components that operate at lower temperatures, for example for the METIS project.[2] The entire cryostat can be freely rotated to allow testing of components in different gravity vectors and to facilitate installation of the components onto the base plate. The cryostat frame is equipped with lockable wheels to allow it to be moved around the lab. The vacuum vessel was designed in-house, with manufacture externally in order to develop work flows relevant for the larger METIS cryostat that is also being developed at ETH.

1.1 Cooler Choice

The chosen cooler was a Sumitomo Heavy Industries SRP-082B2S, a two stage pulse tube cooler. This unit has a nominal performance of 1 W at 4.2 K and 40 W at 45 K, in excess of what is needed for operation at the ERIS wheel test temperature of 70 K, but required for an MLI free design that can operate down to ≈10 K. The large margin at higher temperatures also allows the cryogenic testing of large motors that have a high heat dissipation. A pulse tube cooler was preferred over a moving cold mass cryocooler due to the lower vibration,[3] critical for testing high precision cryo-mechanisms. The cooler was specified with a remote valve unit in order to further reduce the vibration of the cold head. At low temperatures, the cooling power on the second stage is dependent on the heat load on the first stage and the nominal performance data is readily accessible from SHI.[4] For testing of the ERIS wheels at higher temperature, or for modeling cool-down, less data is available

Further author information: (Send correspondence to S.A.M.)
S.A.M.: E-mail: stephen.march@phys.ethz.ch, Telephone: +41 44 632 38 13

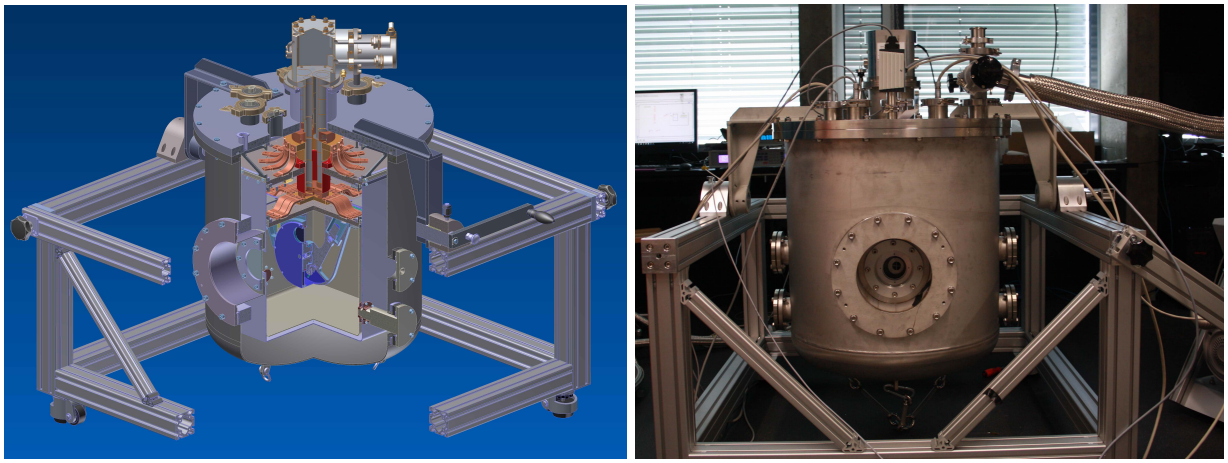

Figure 1. Left: 3D CAD model of the test facility and right a photograph of the finished assembly. Right: Photograph of the completed cryostat. In both images the cryostat is orientated so that the cryocooler has the cold finger pointing down, i.e for when the pulse tube cooler is operational. For opening the vacuum vessel and accessing the cold box the entire cryostat is rotated (by hand) so that components can be easily installed on the cold plate.

and so the fit was conservatively extrapolated. Furthermore, the temperature dependence of the two stages was ignored in order to allow the cooler to be modeled in ANSYS. Thermal network modeling (no 3D geometry) using a custom MATLAB program allowed analysis of the cool-down with the temperature dependence of the two stages. A limitation of this GM-type pulse tube cooler is that the cold tip must point down, as there is a strong dependence of the available cooling power on the inclination angle.

The first stage was connected to the thermal shield and the second stage to the base plate of the cold box. Heaters and temperature sensors were installed close to both the first and second stages. The heaters were independently controlled using a LakeShore 336 to provide good temperature stability and flexibility as to the operating thermal environment.

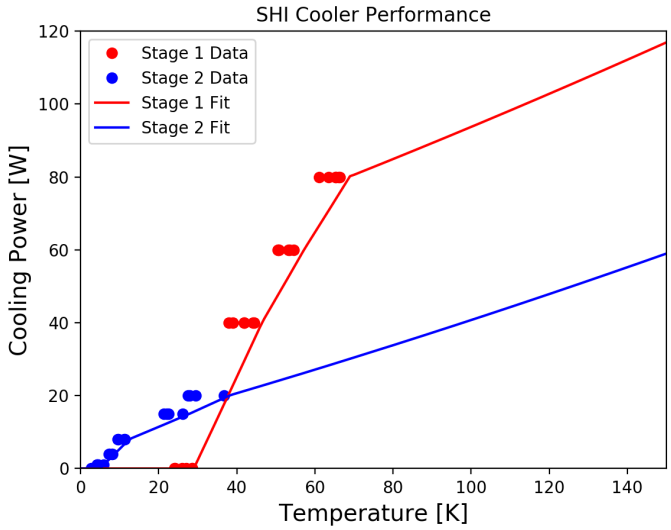

Figure 2. Performance of the SHI cooler. The data at low temperature is from the manufacturer. The conservative fit (piece-wise linear) is for extrapolation to higher temperatures and assumes independence of the two stages. This fit was used for modeling the complete system in ANSYS, including transient analysis.

1.2 Radiation shields and plates

The radiation shields were designed to minimize thermal gradients across the cold box, as well as reducing the heat load on the second stage. The radiation shield was cooled by the first stage of the cryocooler and the cold box by the second stage. An MLI free design was chosen in order to prioritize easy access to the cold box when installing components at the expense of a higher radiation load. The sheets forming the radiation shields and cold box were electro-polished to lower their emissivity. A value of 0.08 was estimated from transient measurements of the cryostat, in-line with values measured by ESO for a similar process.[5]

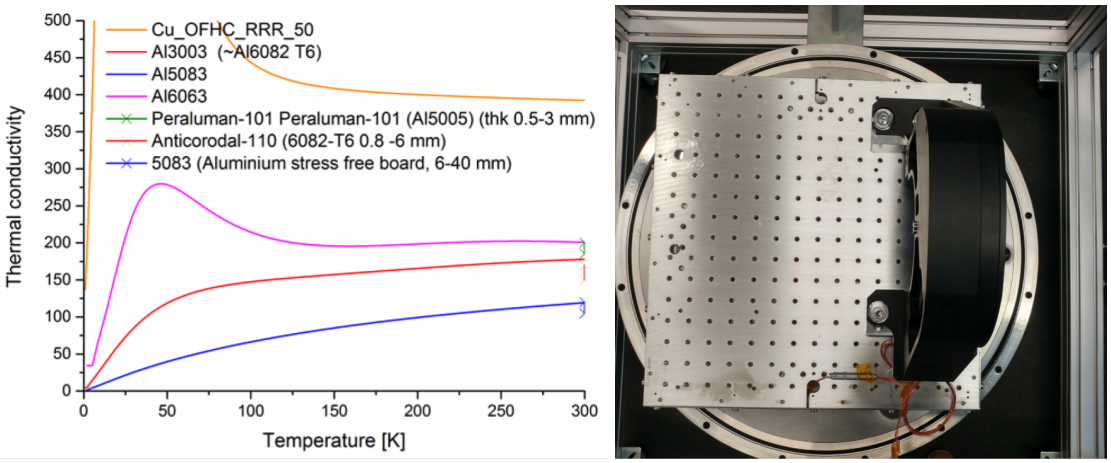

Figure 3. Left: Thermal conductivity of selected materials from NIST at cryogenic temperatures. Room temperature values are also shown for aluminum plates and sheets standardly available at ETH. Right: The Al-6082 base plate of the cold box with it's raster of threaded holes, similar to an optical bench, allows a variety of components to be easily installed.

Due to the large optical aperture, there is a large radiation load through the thermal shield into the cold box. For visible light tests an IR-filter can be installed on the shield, when the radiation load to the component under test must be minimized. The aperture can also be closed completely with a blanking plate for when a window is not required (e.g. for motor performance tests). Aluminum was used due to its ease of machinability, high thermal conductivity, and low cost. Oxygen free copper was considered as an alternative, however, the thermal performance increase did not outweigh the cost penalty. Despite having a lower thermal conductivity than other alloys, Al-6082 was chosen as it can be electro-polished to a higher standard than 5000 series alloys, resulting in a lower radiation load.[6] The mass and thickness penalty for achieving the same thermal resistance is minimal for this cryostat.

The thermal conductivity of the materials available at ETH and cryogenic data is shown in Figure 3. The base plate has a raster of threaded holes, similar to an optical bench, in order to allow a variety of components to be installed in the appropriate configuration Figure 3. The thickness of the base plate is to minimize the thermal gradients and to act as a thermal battery for cryogenic testing with the cryocooler turned off. For example to reduce vibration, or when the pulse tube cooler was not vertically orientated. There is a second plate at the first stage/radiation shield level that is used for attaching the non-isothermal supports as well as other thermal hardware.

1.3 Non-Isothermal Supports

Supports were needed to rigidly hold the cold box and radiation shields to the vacuum vessel flange. As well as being stiff, the supports needed to withstand mechanical loads and minimize the heat leak from the vacuum vessel at room temperature to the cold box at $\approx$10 K. The supports were thermally intercepted at the level of the cryocooler first stage (radiation shield). Fiberglass leaf spring type mounts and also fiberglass tubes were considered for this role. After analysis, a novel design comprising of a fiberglass plate that could be purchased cut-to-shape was chosen. This design provided a frame that was easy to assemble, stiff in any orientation of the

cryostat, yet still had a low heat leak. The design was analyzed using FEA before manufacture and a prototype support underwent a cool-down test.

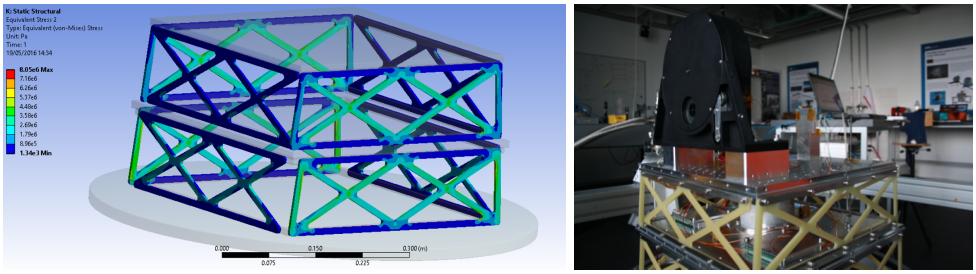

Figure 4. Left: FEA of the supports at the end of cool-down. The stress distribution arises due to the different thermal contraction of the components, with the weight of the cold mass only giving a minor contribution. Right: Photograph of the fiberglass supports when installed in the cryostat. An ERIS wheel (black) is also mounted, in preparation for cold testing.

1.4 Thermal Links

Thermal links are needed for attaching the cryocooler to the cold mass. These links must have a low thermal resistance in order to fully utilize the cooling power of the cryocooler, but also have good flexibility in order to compensate for differential thermal contraction of the cryostat components and to mechanically decouple the cooler. A braid type thermal link was chosen in order to maximize flexibility and ease of manufacture. Foils, which have a lower outgassing surface and a higher packing factor, were investigated but not chosen due to their higher stiffness. The difference in packing factor between a braid type link and a foil type link can be seen in the below photograph (Figure 5).

Material choices for the braids were oxygen Free (OF) copper or Electrolytic-Tough-Pitch (ETP) copper, the foils were additionally available in aluminum. OF copper has superior thermal conductivity at low temperature, however, above ≈100 K the difference is marginal. For the lab cryostat ETP copper was used for cost and availability reasons. The penalty in thermal performance was not an issue for this application and the design allows more braids to be added if required. Nominally 8 braids are required, however, the adapters allow up to 16 to be installed.

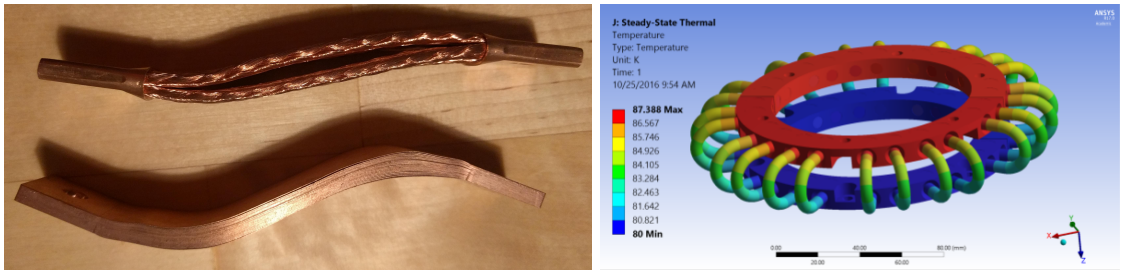

Figure 5. Left: Top a thermal link formed of copper braids and swaged end caps, bottom a thermal link formed of pressed copper foils. Right: Thermal analysis of a low thermal resistance thermal link based on previous ETH designs. The copper braids are electron beam welded into the supporting rings, which are split to facilitate installation. The design uses oxygen free copper and is particularly suited to low temperature use, however, a lower cost alternative was selected for this cryostat.

Typical methods of constructing thermal links are detailed in[78] . ETH has experience in making low temperature thermal links where the braids are electron beam welded to the adapter for low thermal resistance. A possible design was investigated for this cryostat, see Figure 5, however, the chosen option was swaging as it is lower cost than electron beam welding and can provide better flexibility than soldered options. The braids,

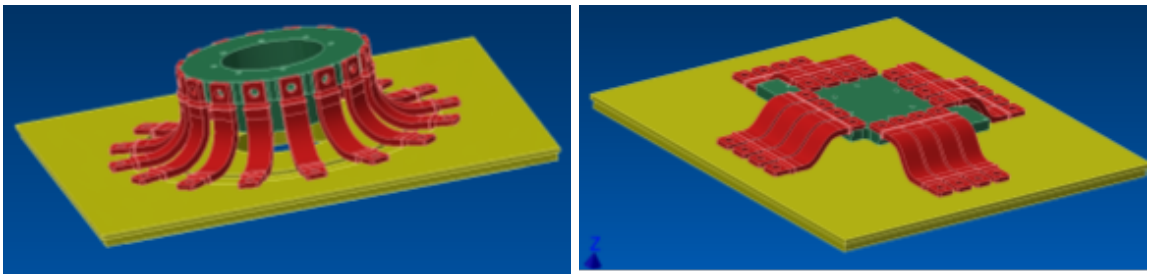

Figure 6. Left: Thermal link layout for attaching the first stage to the radiation shields. Right: Thermal link layout for attaching the second stage to the cold box. In both cases the braids and end caps are shown in red, the plate to which they attach in yellow, and the oxygen free copper adapter to the cold finger in green.

including end caps, were commercially sourced in a standard size to reduce costs. The overall design of the thermal links allow a varying number of braids to be installed to adjust the thermal performance.

A CAD model (Figure 6) shows the thermal links for the two stages. There are two different setups, one with a degree bend in the straps (1^{st} Stage), the other with a flat S-shape" strap (2^{nd} Stage). The straps (in red) are used to transfer heat from a fixed bus (in green) to a plate (in yellow). The nominal operating condition is achievable with 8 straps/stage, however, up to to 16 straps/stage can be used to decrease the thermal resistance. For example, if a good thermal contact can not be achieved or degrades over time.

2. THERMAL PERFORMANCE

The thermal performance of the cryostat during the design phase using ANSYS for modeling the 3D geometry and a custom MATLAB program for nodal network analysis. The nodal network analysis allowed fast calculation of the thermal performance, including transients, which allowed a wide parameter space to be investigated and critical values (e.g. thermal resistances) to be optimized.

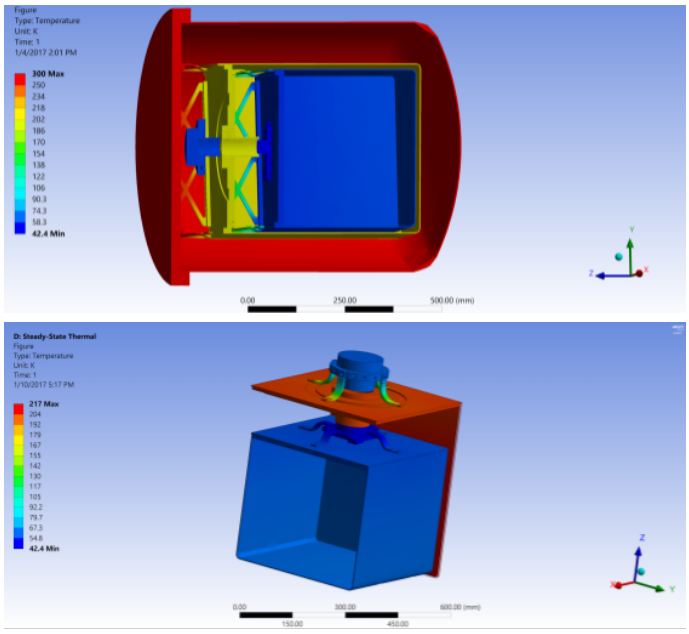

Figure 7. Top: Example temperature distribution in the cryostat with a shield unpolished shields (emissivity of 0.3) and only 4 copper braids installed in each thermal link. Bottom: Close up of the temperature distribution on the cold box.

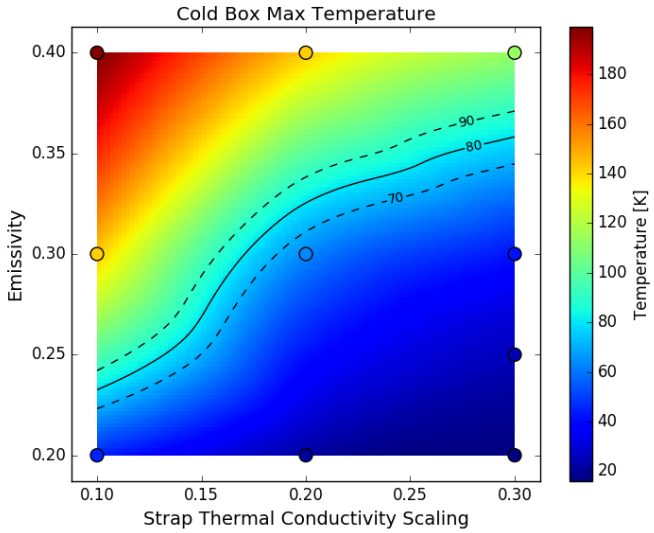

Figure 8. Results of a parametric analysis performed in ANSYS on the full geometry of the cryostat. The emissivity of the shields was varied over a likely range and the conductivity of the links scaled to account for variation contact resistance and in material properties. Even with degraded shields and high thermal resistance thermal links the ERIS requirement of 70 K can be met, with likely properties resulting in a cold box temperature of ≈10 K.

A large challenge in analyzing cryogenic device is in the estimation of material properties, emissivity, and thermal contact conductance. Material properties can vary by several orders of magnitude over the operating temperature range, have variation even at room temperature, and data may not be available at low temperature. Thermal contact conductance can also vary considerably and strongly depends on the joint design and interface conditions. Some information on copper to copper joints at cryogenic temperatures can be found in.[9] The radiation load varies with the emissivity and as this cryostat is MLI free, the variation was estimated to be between 0.3 for unpolished aluminum and 0.1 for polished aluminum. The design and analysis focused on ensuring that the required performance could be met, even with uncertainties in thermal conductivity, contact conductance, and emissivity.

An example temperature distribution of the cryostat in shown in Figure 7. In this setup, all emissivities were set to 0.3 (i.e. not polished), the thermal contact conductance between the thermal links was assumed to be perfect, but only 4 instead of the nominal 8 braids were used. The cabling load, which is intercepted at the first stage of the cooler, was ignored as it is negligible compared to the radiation load. The heat leak through the supports was included. In this analysis the cold box temperature was estimated to be ≈45 K with a negligible gradient around the cold box. Similar analyses were performed over a wide range of parameters and were used for a parametric study, to confirm design choices, as well as to estimate if the desired 10 K temperature could be reached.

The results of a parametric analysis of the cold box temperature as a function of the thermal link performance and emissivity of the shields in shown in Figure 8. The analysis showed that the 70 K requirement for the ERIS test could be achieved without polishing the shields and with the thermal conductivity of the thermal links scaled to 20% of their nominal value. With polished shields (emissivity of 0.1) and thermal links with their nominal material properties the desired temperature of 10 K was shown to be achievable.

3. COMMISSIONING

The test facility was successfully commissioned in 2017. The vacuum pump down speed and hold time was fast and allows the pump to be turned off during measurements sensitive to vibrations. During the first few cool-downs, the cryocooler was only turned on during lab operating hours. However, when cold the cryocooler was run continuously. A control system that allows push button cool-down and autonomous operation is planned.

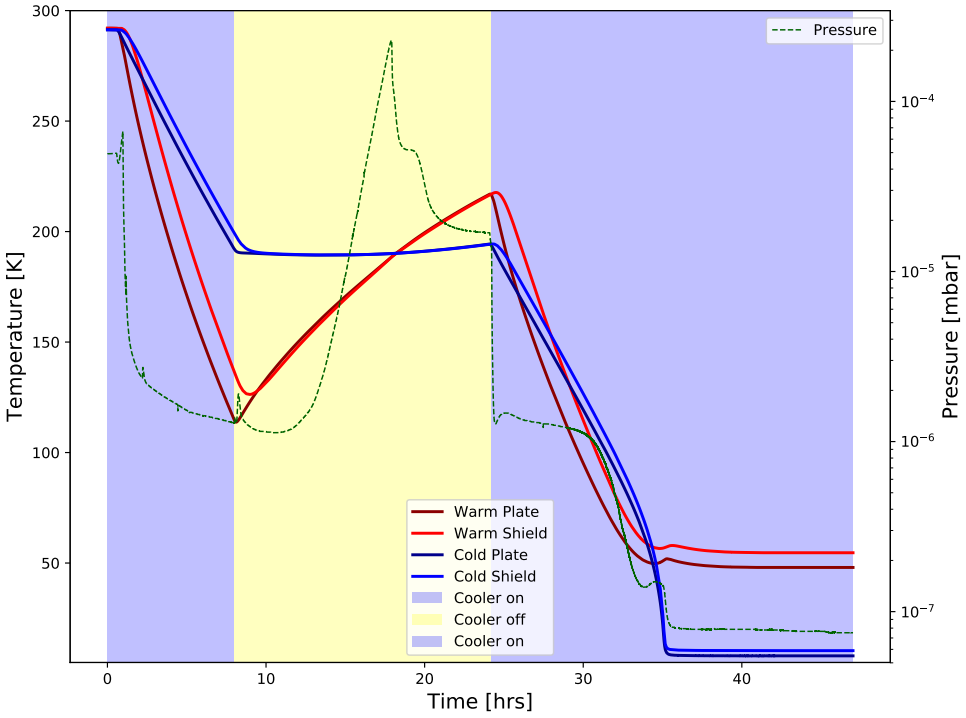

Figure 9. First cool-down of the "Silver Bell" test facility in 2017. The cool-down progressed smoothly with a minimum temperature of 8 K being achieved. For the initial cool-down, the cryocooler was only operated during the working day and was turned off over night. After several successful runs the cryocooler is now run continuously during a cool-down.

Due to the large amount of cooling power on the first stage, the warm plate and shield cool-down rapidly to about 50 K, followed by the cold plate and shield that are cooled by the second stage. At lower temperature the cool-down rate of the cold box (cold plate and shield) accelerates before achieving a temperature of 8 K. The temperature of the cold box can be set depending on the test requirements and at 70 K (the test temperature of the ERIS wheels) the measured thermal gradients across the cold box can be reduced to zero by independently controlling the warm plate and shield.

Heaters and temperature sensors were installed close to both the first and second stages. The heaters were independently controlled using a LakeShore 336 to provide good temperature stability and flexibility as to the operating thermal environment. Adequate thermal contact conductance could be achieved without the use of indium. Apezion grease was only used for the contacts to the cryocooler (joints that remain closed) and was not needed for the frequently opened contacts between the shields and plates.

4. CONCLUSION

A multi-purpose cryogenic test facility for astronomical instrumentation was designed by ETH Zurich for the primary purpose of testing the ERIS wheels. The facility has a generic application portfolio and can be used for other development projects, in particular cryo-mechanisms. The test facility was successfully commissioned in 2017, reaching a coldest temperature of ≈8 K. At 70 K, the ERIS wheel test performance test temperature, there is good thermal stability and ample cooling power available. Measurements so far in the "Silver Bell" include characterization of cryogenic stepper motors and performance tests of the Pupil- and Filter-Wheel and the Aperture-Wheel mechanisms for the NIX camera of the VLT/ERIS instrument.[1] The design, manufacture,

and operational experience of the facility also contributes to the METIS cryostat and other ETH projects focused on IR astronomy. The test facility is now available for testing a wide range of cryogenic devices.

ACKNOWLEDGMENTS

Thanks to Evert Nasedkin for assistance in assembling and commissioning the cryostat. The stepper motor tests were performed by Evert as part of his semester project. Thanks to Walter Bachmann (ETH Engineering Office) for helpful discussions during the design phase and to the ETH Workshop for manufacturing of the facility. The financial support of the ETH Physics Department is greatly acknowledged.

REFERENCES

[1] Glauser, A. M., Pearson, D., Macintosh, M., Taylor, W., March, S. A., Feuchtgruber, H., Rau, C., Davies, R., Quanz, S., and Schmid, M. H., "Development of cryogenic mechanisms for the VLT/ERIS instrument," in [*Astronomical Telescopes and Instrumentation*], 10702–109, SPIE, Austin (2018).

[2] Brandl, B., "Status of the mid-infrared elt imager and spectrograph metis," in [*Astronomical Telescopes and Instrumentation*], 10702–66, SPIE, Austin (2018).

[3] Tomaru, T., Suzuki, T., Haruyama, T., Shintomi, T., Yamamoto, A., Koyama, T., and Li, R., "Vibration analysis of cryocoolers," *Cryogenics* **44**(5), 309–317 (2004).

[4] Industries, S. H., "RP-082B2 4K Pulse Tube Cryocooler Series." http://www.shicryogenics.com/products/pulse-tube-cryocoolers/rp-082b2-4k-pulse-tube-cryocooler-series/ (2012).

[5] Lizon, J.-L., "Cryogenics and Vacuum," in [*ESO Training Course*], ESO, Granada (2016).

[6] Poligrat GmbH, "Electro-polishing of Aluminum Alloys." Private communication (2016).

[7] Williams, B. G., Jensen, S. M., and Batty, J. C., "Advanced solderless flexible thermal link," *SPIE* **2814**, 209–216 (oct 1996).

[8] "Solderless flexible thermal links," *Cryogenics* **36**(10), 867–869 (1996).

[9] "Thermal contact conductance of demountable in vacuum copper-copper joint between 14 and 100 K," *Review of Scientific Instruments* **83**(3) (2012).